Structure of pseudomorphic and reconstructed thin Cu films on Ru(0001)

H. Zajonz,[1,*] A. P. Baddorf,[2] Doon Gibbs,[1] and D. M. Zehner[2]
[1]*Department of Physics, Brookhaven National Laboratory, Upton, New York 11973-5000*
[2]*Solid State Division, Oak Ridge National Laboratory, Oak Ridge, Tennessee 37831-6057*
(Received 17 March 2000)

The structure of strained Cu films deposited on Ru(0001) surfaces at 720 K was investigated by x-ray diffraction techniques. Our analysis shows that a single Cu monolayer adopts a pseudomorphic structure with the first three interlayer spacings significantly relaxed. The two-layer structure consists of a commensurate, uniaxially modulated stripe-phase reconstruction. Modeling the diffraction intensities through application of simulated annealing techniques, together with least-squares refinement, has led to a crystallographic description of this structure in terms of a set of three-dimensional modulation functions. We find that the reconstruction persists through both Cu layers, and leads to relaxation of the Cu and Ru interlayer spacings. We also calculate the average strain distribution as a function of position across the unit cell.

INTRODUCTION

The bimetallic interface comprised of a thin Cu film grown on a Ru(0001) substrate has been a focus of discussion of epitaxial strain accommodation for nearly 20 years.[1–21] The interest in this system derives in part from the catalytic properties of the Ru(0001) surface, which supports hydrocarbon conversion reactions.[22–25] Indeed, its catalytic activity can be enhanced by as much as a factor of 40 in the presence of a submonolayer coverage of Cu.[23] Generally, the catalytic properties of Cu on Ru(0001) are believed to originate in the modification of the electronic band structure induced by the interfacial strain.[26–28] The bulk near-neighbor spacing of Cu is smaller than that of Ru by 5.8% at room temperature, which leads to a net tensile strain at the interface.

There is also basic interest in this system concerned with characterizing the interfacial structures that occur versus Cu coverage and substrate temperature. Earlier scanning tunneling microscopy and low-energy electron diffraction (LEED) studies have shown that the first Cu monolayer (ML) grows pseudomorphically on Ru(0001), followed by the formation of a uniaxially compressed stripe phase upon further Cu deposition.[7,10,12,15–17,21] At higher Cu coverages, bulklike Cu islands form in coexistence with the stripe phase.[8,17,21] Our own recent x-ray scattering studies have probed the real-time growth of these structures, and uncovered a surprising property of the stripe-phase wave vector, namely, that it locks to the substrate with unit cell size depending on temperature.[21] The growth properties of these thin films, and their dependence on temperature, continue to challenge current theories.[29]

In spite of the importance of the pseudomorphic and stripe phases, there remains a serious lack of detailed, structural information concerning their properties, particularly of the buried layers. It is not clear from the literature, for example, whether the stripe phase for two layers of Cu on Ru exists only within the topmost Cu layer or involves a bilayer reconstruction. Likewise, very little is known about the response of the underlying Ru substrate to Cu adsorption at any coverage. This kind of information is crucial to an overall understanding of the structure, and adds insight to the energetics of strain evolution at interfaces. In this regard, it is worth commenting that the absence of such information is not as surprising as it might at first seem. Scanning techniques are limited to probing the topmost layer, while diffraction studies have been limited by the large number of parameters required to describe the stripe modulation. The latter problem can be simplified by the introduction of a suitable set of modulation functions with a smaller number of parameters; however, it is still difficult to find global optima since the parameters tend to be strongly correlated. Progress has been made in this area by the application of statistical methods, such as simulated annealing. Nevertheless, the impact of these methods on x-ray surface crystallography has been limited to date.

In this paper, we describe detailed x-ray scattering studies of the structure of the one- and two-layer reconstructions of Cu on Ru(0001) at 720 K. The crystallographic analysis of the data was performed using both least-squares refinement and simulated annealing techniques. Our results confirm the pseudomorphic character of the single-monolayer structure, but extend that picture to include the relaxation of the Cu and Ru interlayer spacings. For the commensurate, stripe-phase reconstruction, we derived a set of three-dimensional modulation functions, which show that the reconstruction involves a uniaxial modulation of both Cu layers. The displacements transverse to the modulation direction are approximately sinusoidal and only slightly out of phase within the two layers. The longitudinal modulation is asymmetric across the unit cell and different for the two layers. On the basis of these results, we have calculated the average strain distribution across the unit cell. Interestingly, it is inhomogeneous and appears smaller on average in the top Cu layer than at the interface. Finally, we find that the Ru substrate is laterally undistorted and exhibits only small relaxations of the interlayer spacings near the interface.

EXPERIMENT

The x-ray experiments reported in this paper were performed using beam line X22C at the National Synchrotron Light Source (NSLS). This beam line is equipped with a bent, cylindrical, platinum-coated focusing mirror (spot size $\sim$1 mm) and a Ge(111) double-crystal monochromator. In the present experiments we used monochromatic x rays with an energy of 10.5 keV. Preceding the x-ray experiments, the

Ru(0001) crystal (diameter 6 mm and thickness 1.5 mm) was mounted in the ultrahigh vacuum (UHV) surface diffractometer,[30] which is operated at a base pressure below 1×10^{-10} Torr. Surface preparation involved sputtering at 300 K with 1 keV Ar ions followed by repeated cycles of oxygen annealing to remove carbon.[31,32] The sample was heated from the back by electron bombardment from a tungsten filament, and the temperature was measured by a WRe5%-WRe26% thermocouple. Cu was evaporated onto the Ru(0001) surface from a resistively heated Knudsen cell to produce coverages of one or two layers. The deposition rate was calibrated from oscillations of the x-ray reflectivity observed at the (0001) position and was set at about 0.1 ML per minute. Using an Auger electron spectrometer equipped with a cylindrical mirror analyzer, we found that no traces of contaminants were present on the crystal surface to within the sensitivity of the instrument (~0.01 ML). The surface orientation of the crystal was polished to within 0.1° of its crystallographic (0001) plane. The bulk mosaic width was about 0.07°.

The substrate temperature was fixed at 720 K. This temperature was chosen based on our earlier studies, which showed that the domain size of the stripe phase reached a maximum of ~800 Å at this temperature. In addition, we found that the widths of Cu superstructure reflections broadened substantially upon cooling to room temperature.[21] A total of 960 integrated intensities were measured in the *z*-axis geometry by rotating the sample around its surface normal and subtracting the diffuse background signal.[33] This set of reflections includes symmetry-equivalent data taken for both the pseudomorphic 1 ML structure and the bilayer stripe-phase reconstruction. Symmetry reduction of the data set resulted in 477 nonequivalent reflections. The error of the diffracted intensities was estimated from the measured reproducibility of symmetry-related reflections, and produced an internal R value of 17% based on $|F|^2$ for all reflections. The data were corrected for polarization, Lorentz factor, active sample area, and the resolution function of the instrument. For the analysis of the pseudomorphic structure (1 ML), 84 data points were acquired along the $(0,0,0,L)$ and the $(1,0,-1,L)$ crystal truncation rods (CTR's).[34] For the reconstructed bilayer structure we obtained a set of 118 superstructure reflections, including 50 in-plane and 68 superstructure rod reflections. In addition, 241 CTR data points were measured along the $(0,0,0,L)$, $(1,0,-1,L)$, $(2,0,-2,L)$, $(2,1,-3,L)$, $(1,2,-3,L)$, and $(1,1,-2,L)$ CTR's. Rod data were taken up to a maximum normal momentum transfer of $Q_z=3.67$ Å^{-1} which is equivalent to 2.5 reciprocal lattice units of c^*. These results are presented in the conventional crystallographic notation of the Ru substrate with the inplane lattice constant a equal to 2.706 Å at room temperature. The lattice constant normal to the surface c is equal to 4.282 Å.

RESULTS AND DISCUSSION

1 ML of Cu on Ru(0001)

The in-plane diffraction pattern of the Cu monolayer on Ru(0001) showed no evidence of additional superstructure reflections for any substrate temperature up to 720 K. This implies that neither the substrate nor the adlayer exhibits lateral relaxations, including the possibility of an ordered reconstruction. The only deviations of the structure from ideal termination that then remain to be investigated are the registry, interlayer relaxations, and Debye-Waller factors of the surface layers. This information is contained in the intensities distributed along the crystal truncation rods.[34] Specifically, the superposition of diffraction amplitudes from the relaxed surface and from the undisturbed Ru can interfere, thereby altering the intensities along the $(0,0,0,L)$ and $(1,0,-1,L)$ rods. Our experimental results and analysis for a monolayer of Cu on Ru(0001) are shown in Fig. 1. The diamonds represent the experimental data and the solid line shows the best fit based on a minimization of the weighted residual $R_W(\log_{10}[I])$ with respect to the logarithm of the measured intensity.[35] To obtain this fit, the first three layer distances, a Debye-Waller factor for the topmost two layers, and an overall scaling factor were adjusted in a least-squares refinement.

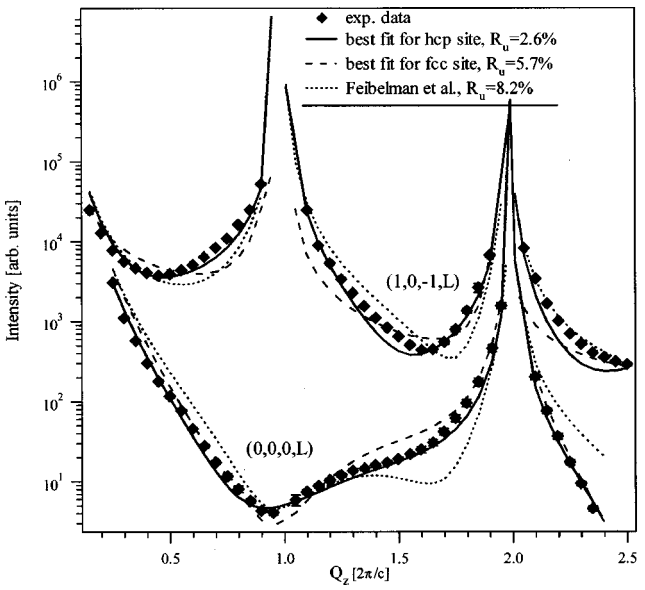

FIG. 1. $(1,0,-1,L)$ and $(0,0,0,L)$ CRT's for a monolayer of Cu on Ru(0001). The diamonds represent the measured intensities; the solid line is the best fit to the data based on a Cu(1×1)-hcp layer with interlayer relaxations (see text). The dashed line shows the best fit of a model in which Cu resides in fcc sites. The model of an earlier LEED study (Ref. 13) is shown by the dotted line.

The best fit gave a weighted residual of R_W of 2.6%. The variation of the off-specular $(1,0,-1,L)$ rod intensities confirms hcp stacking of the Cu layer on Ru(0001). This result is in agreement with earlier LEED measurements,[13] and verifies a pseudomorphic arrangement (Fig. 2). From this it follows that a monolayer of Cu on Ru(0001) is 11% less dense than bulk Cu, and therefore that a tensile strain is present at the surface. For comparison, the dashed line in Fig. 1 shows the best fit for a model with Cu in fcc positions on Ru(0001). The fitted intensity distribution along the $(1,0,-1,L)$ rod clearly deviates from the experimental data ($R_W=5.7\%$) making fcc stacking of the Cu layer unlikely.

The analysis of the $(0,0,0,L)$ and $(1,0,-1,L)$ rods also allows the determination of interlayer spacings at the surface with respect to Ru bulk. Table I lists the interlayer distances obtained in this study together with the findings of earlier diffraction studies of this system. The table also includes the

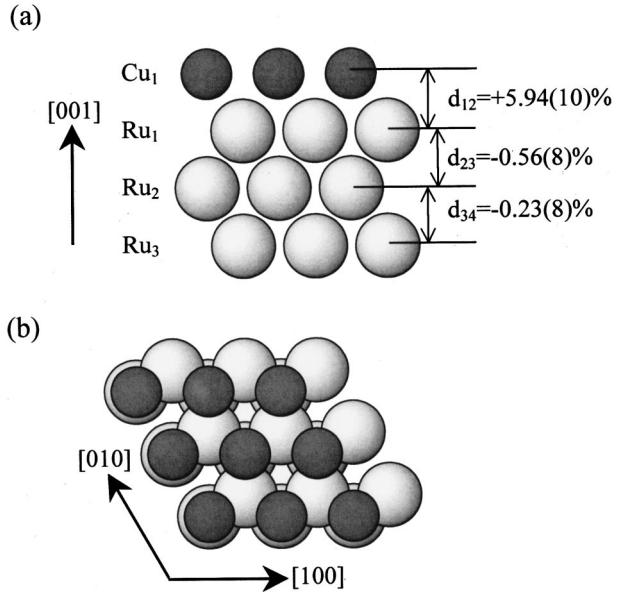

FIG. 2. Side (a) and top (b) view of the hcp Cu/Ru(0001)-(1×1) structure.

interlayer spacings of the clean, relaxed Ru(0001) surface obtained by both LEED and x-ray scattering.[13,36]

The average metallic radius of a Cu atom is 5.8% smaller than that of Ru. It follows that in a hard-sphere model of the structure a Cu atom resides 4.1% deeper in the hollow site of the Ru(0001) substrate than would a Ru, assuming there are no relaxations present at the surface. With respect to this idealized spacing, we find that the distance between the Cu layer and the topmost Ru layer is expanded by 5.94(1)%, as indicated by the label d_{12} in Fig. 2(a). In contrast, the spacings of the following two layers are contracted by 0.56(8)% for d_{23} and by 0.23(8)% for d_{34}. Relaxation of subsequent Ru layers did not significantly improve the fit to the model, suggesting that these layers adopt bulk Ru spacings.

Our model also includes a root mean squared (RMS) vibrational amplitude for the topmost two layers. For Cu, we find a surprisingly small RMS amplitude of 0.04(2) Å which implies a rather smooth surface and a strong Cu-Ru bonding. The interfacial Ru layer has a RMS amplitude of 0.09 Å, which is within 5% of its bulk value at 426 K.[37]

The model deduced in the LEED study noted above[13] is represented by dashed lines in Fig. 1. Its residual R_w of 8.2% implies that it does not accurately describe our data. Specifically, it yields an expansion of the Cu-Ru spacing d_{12} by only one-fourth of our observation, and otherwise gives different relaxations of the first and second Ru layers. With reference to a clean, relaxed Ru(0001) surface,[13,36] the LEED study implies an additional contraction of 0.6–0.7 % of the Ru-Ru interlayer distance upon Cu deposition. In contrast to that, we find that the first Ru interlayer distance expands by 1.5–1.6 %. This expansion is expected in charge-smoothing and bond-order models,[38] and is also in agreement with linearized augmented plane-wave calculations. However, the calculations predict only a 0.5% expansion of the Cu-Ru spacing.[13] It should be noted that this prediction does not consider the effect of temperature on the structure, which could be a reason for the discrepancy.

It is worth remarking that the observed pseudomorphic structure is accompanied by a drop of the work function by 0.32 eV upon Cu deposition.[17] This implies that the large Cu-Ru spacing is related to the change of the electronic band structure at the surface. In this regard, it has been suggested by angle-resolved ultraviolet photoemission studies and surface linearized, augmented plane-wave calculations that the Cu 3d and Ru 4d states overlap sufficiently in the pseudomorphic regime to introduce a ''true'' interface state.[39] This relatively strong bonding to the Ru substrate could explain the formation of a strained but stable pseudomorphic overlayer. The idea of hybridized d bands is also supported by thermal desorption spectroscopy, which showed that the Cu-Ru binding energy for the first monolayer is significantly higher than that for subsequent Cu layers.[40]

Two layers of Cu on Ru(0001)

The deposition of an additional Cu layer to the single-monolayer system leads to a stripe-phase reconstruction as has been described earlier.[7,10,15–17] Figure 3 shows a schematic representation of the diffraction pattern of the bilayer Cu reconstruction on Ru(0001) as observed in our x-ray experiments at $T=720$ K. The in-plane diffraction pattern consists of rows of superstructure reflections with detectable intensities close to the Ru bulk Bragg reflections, consistent with a uniaxial reconstruction. The underlying hexagonal symmetry of the Ru(0001) surface implies that there are three equivalent in-plane directions, and therefore three do-

TABLE I. Surface x-ray diffraction (SXRD) (Ref. 36) and LEED (Ref. 13) results.

	1 ML Cu/Ru(0001)		Clean Ru(0001)	
	This study $T=720$ K (SXRD)	Ref. 13 $T=293$ K (LEED)	Ref. 36 $T=293$ K (SXRD)	Ref. 13 $T=293$ K (LEED)
Cu layer orientation	hcp	hcp		
$\Delta d_{1\text{-}2}$ Cu_1-Ru_1 (%)	+5.94(10)	+1.5		
$\Delta d_{2\text{-}3}$ Ru_1-Ru_2 (%)	−0.56(8)	−2.8	−2.20(1)	−2.1
$\Delta d_{3\text{-}4}$ Ru_3-Ru_4 (%)	−0.23(8)	0.0	−0.40(1)	−0.1
$\Delta d_{4\text{-}5}$ Ru_4-Ru_5 (%)	0.00	+0.5	+0.30(6)	+0.5
$\Delta d_{5\text{-}6}$ Ru_5-Ru_6 (%)	0.00	+0.5	0.00	−0.1
$\Delta d_{6\text{-}7}$ Ru_6-Ru_7 (%)	0.00	−0.7	0.00	−0.6
RMS Cu1 (Å)	0.04(2)			
RMS Ru1 (Å)	0.09(3)		0.06(4)	

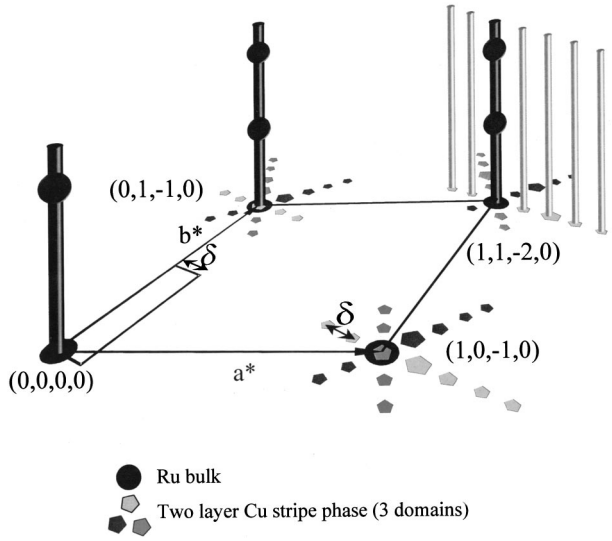

FIG. 3. Schematic diffraction pattern for the three observed domains of the Cu bilayer reconstruction on Ru(0001). The small rectangle represents the surface unit cell. A detailed description can be found in the text.

mains of the reconstruction on a Ru terrace. Each of these produces additional reflections around the bulk peaks of the Ru substrate. The intensity distribution along the superstructure rods is continuous, as expected from a two-dimensional structure. The CTR's occur with the in-plane periodicity of the Ru Bragg reflections and connect them perpendicular to the surface, as is also shown in Fig. 3.

The spacing between the superstructure reflections along the $[2\bar{1}0]$, [110], and $[1\bar{2}0]$ directions (see Fig. 3) defines the incommensurability δ of the Cu bilayer with respect to the Ru substrate. Figure 4 displays a radial scan through the Ru (1,0,−1,0.15) CTR showing the principal Cu peak together with Cu satellite reflections up to third order. It should be mentioned that δ is not constant during the growth of the second Cu layer and does not appear to correspond simply to a commensurate value. Rather, upon completion of the second Cu layer, a small contraction of about 0.02 Å between Cu atoms is observed, and δ locks to a commensurate value of $\frac{1}{16}$ at 720 K.[21] The superstructure cell is described by the

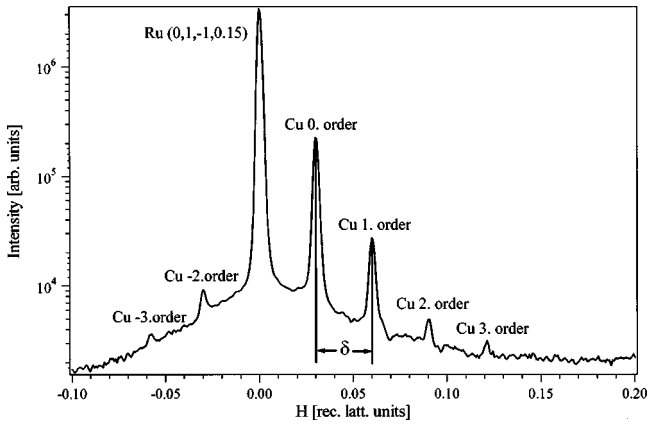

FIG. 4. Radial scan through the (0,1, −1,0.15) CTR of the stripe phase showing the Ru CTR, the principal Cu reflection (zeroth order), and higher-order satellites of the modulated reconstruction.

matrix $\binom{16\ 0}{1\ 2}$. This matrix specifies a rectangular cell in which 17 Cu atoms lie on top of 16 Ru atoms along the [100] direction. The superstructure lattice vector **b** is enlarged by a factor of $\sqrt{3}$ and rotated by 30° with reference to the corresponding hexagonal lattice vector of the Ru(0001) substrate. The periodicity along **a** is increased by a factor of 16, which defines the period of the bilayer reconstruction (see Fig. 5 below).

A three-dimensional description of the modulated surface generally leads to plane symmetry $P1$. In the present case, there are potentially 164 atoms in the surface unit cell, each with three positional parameters x, y, and z, when relaxations of up to five atomic layers are assumed. The net result is that approximately 492 components are needed to describe the structure. A least-squares fit with such a large number of parameters requires a very large data set if the goal is the determination of a unique model. This is a common problem in x-ray surface diffraction, although reliable structural models have been derived with overdetermination by up to a factor of 4.[41] In the present case, the required 2000 data points could not be collected because the intensities of the higher-order Fourier components of the structure drop rapidly toward zero in the accessible range of reciprocal space. This is an intrinsic property of many modulated structures.[42] We were therefore compelled to reduce the number of free structural parameters by introducing a set of modulation functions. These functions describe the spatial displacement of the atoms starting from an unmodulated atomic arrangement in which 17 Cu atoms lie parallel to 16 Ru atoms along the [100] direction. The final model is derived by adding the value of a specific modulation function $f_x(x)$, $f_y(x)$, and $f_z(x)$ to the corresponding position component x, y, and z of each atom. The argument x in $f(x)$ defines the position along the lattice vector **a** that points in the direction of the modulation. A set of periodic functions that proved to be suitable for the present problem is

$$f_x(x)=a_{1,1}\sin(2\pi x+p_{1,1})+a_{1,2}\sin(3\pi x+p_{1,2})+a_{1,3}\sin(4\pi x+p_{1,3}), \tag{1a}$$

$$f_y(x)=a_{2,1}[1-\cos(2\pi x+p_{2,1})]+a_{2,2}[1-\cos(4\pi x+p_{2,2})], \tag{1b}$$

$$f_z(x)=a_{3,1}[1-\cos(4\pi x+p_{3,1})]+a_{3,2}[1-\cos(8\pi\cdot x+p_{3,2})]. \tag{1c}$$

These Fourier series can be truncated after the second or third element depending on their accuracy. The matrices

$$A=\begin{pmatrix} a_{1,1} & a_{1,2} & a_{1,3} \\ a_{2,1} & a_{2,2} & 0 \\ a_{3,1} & a_{3,2} & 0 \end{pmatrix} \quad \text{and} \quad P=\begin{pmatrix} p_{1,1} & p_{1,2} & p_{1,3} \\ p_{2,1} & p_{2,2} & 0 \\ p_{3,1} & p_{3,2} & 0 \end{pmatrix}$$

contain the amplitudes and phases of the Fourier components, respectively. They represent the parameters that ultimately determine the modulated structure. An independent set has been assumed for each modulated atomic layer.

From this we obtain a diffraction amplitude for the modulated superstructure which can be written as

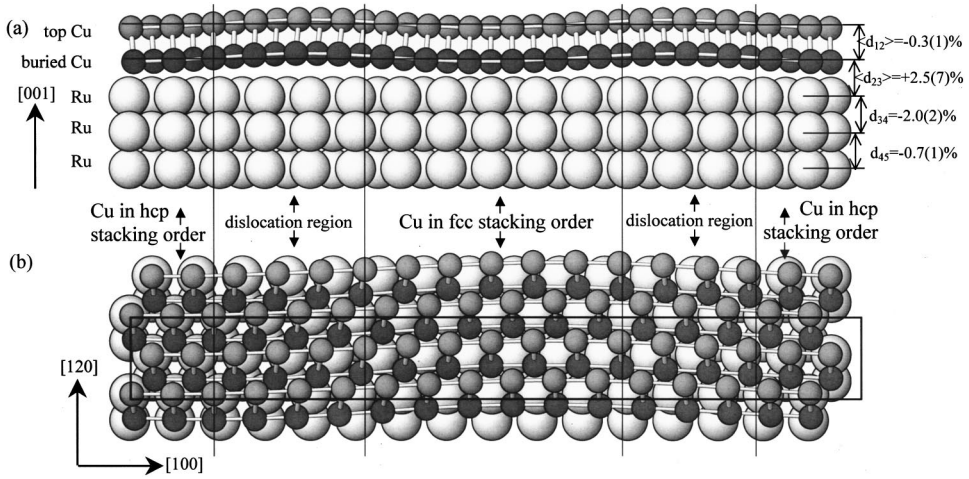

FIG. 5. Structure of the stripe phase. (a) shows the side and (b) the top view of the bilayer reconstruction. The rectangle in (b) represents the superstructure cell.

$$F_{\mathrm{surf}}(hkl)=\sum_{n} f_n(hkl) \times e^{2\pi i\{h[x_n+f_x(x_n)]+k[y_n+f_y(x_n)]+l[z_n+f_z(x_n)]\}}. \quad (2)$$

The indices h, k, and l are the components of the reciprocal lattice vector for a specific reflection. $f_n(hkl)$ is the form factor that describes the scattering of the nth atom with reference to a particular wave vector. (x_n, y_n, z_n) is the coordinate of the nth atom relative to the unmodulated layer.

The analysis was performed with ''very fast simulated reannealing'' algorithms[43] in combination with least-squares refinement techniques. Simulated annealing is well suited to finding the best global fit to a nonlinear function in a multidimensional parameter space.[43,44] Its primary advantage is its ability to move away from the local optima of the cost function. Thus, its capacity to find the global optimum is not confined to the initial conditions, which are given by the start model. Since it is a statistical method, it is model independent in principle but the adjustable parameters can be constrained to remain within the limits for which a realistic solution can be expected.

Fitting

We now turn our attention to the details of the refinement. In order to obtain a model for the stripe phase, the calculations were carried out using all 118 independent superstructure and 241 crystal truncation rod reflections simultaneously. Since CTR data are the result of a coherent superposition of bulk and superstructure scattering, they introduce a phase contrast, which is very sensitive to relaxations of the superstructure. The combination of superstructure and CTR data then permits finer distinctions to be made among different models and enhances the overall reliability of the analysis. Due to the presence of steps, the surface exhibits a total of six rotational domains, which required incoherent intensity averaging for overlapping CTR reflections. Incoherent averaging for superstructure reflections involved only a 180° rotated domain of the modulated overlayer. The fitted parameters included 24 coefficients to describe the modulation of the Cu bilayer, the four topmost layer distances, two scaling factors for in-plane and out-of-plane data, and a roughness parameter β:[34] 31 parameters in total. The parameters were first estimated using our adapted simulated reannealing calculations and then refined with a least-squares program. To avoid the dominance of strong CTR reflections with their relatively small errors close to the Bragg peaks during the refinement, we minimized a weighted residual with respect to the logarithm of the measured intensity.[35] Our best fit resulted in $R_w(\log_{10}[I]) = 3.4\%$.

The resulting model of the Cu stripe phase is shown in Fig. 5. The upper part of the figure displays a side view (a), whereas the bottom part (b) presents a top view with the superstructure cell outlined. One of the most striking features of the reconstruction is its persistence through both Cu layers. This implies that the formerly pseudomorphic Cu monolayer increases its density by one extra atom for every 16 Ru atoms along [100] in order to accommodate the tensile strain at the interface. Interestingly, adding in-plane modulation to the Ru layers did not improve the fit.

Figure 6 displays the details of the refined modulation functions $f_x(x)$, $f_y(x)$, and $f_z(x)$ for the top Cu layer (a) and for the buried Cu layer (b), in Fig. 5. These functions trace the atomic displacements with reference to an unmodulated structure as a percentage of the corresponding superstructure lattice constants. Table II lists the resulting coefficients defined in Eqs. 1(a)–1(c). Referring to Fig. 6, the transverse displacements $f_x(x)$ and $f_y(x)$ in each layer are slightly out of phase. $f_z(x)$ describes the corrugation of the Cu layers as they follow the Ru surface potential, rising from hollow sites to bridge sites (and back) along [100]. During the refinement of the corrugation function, it became clear that the coefficients for these layers are strongly correlated. Therefore, we refined the corrugation of only one Cu layer and used the resulting parameters for both. The maximum vertical displacement caused by the corrugation amounts to 12% of the Ru c lattice constant. The function $f_y(x)$ describes an in-plane displacement of Cu chains by up to 18% of the superstructure lattice constant along [120], with a modulation period twice that of the corrugation. The pattern that emerges from these results involves transverse displacements of all the Cu atoms from hcp sites of the Ru substrate to fcc sites as one travels along the [100] direction, thereby producing stripes (Fig. 5). Between the stripes are dislocation regions in which the Cu atoms reside in quasibridge sites.

The longitudinal modulation $f_x(x)$ along [100] is different for the two layers, involving displacement amplitudes of up to 0.6% for the buried layer and 0.3% for the top Cu layer, as calculated with respect to the superstructure lattice constant a

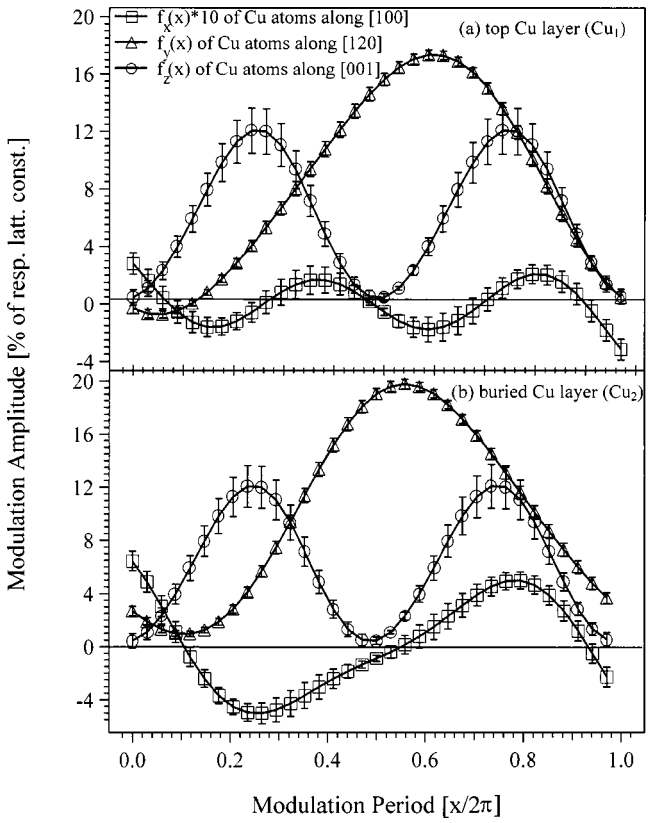

FIG. 6. Modulation functions of the top Cu layer (a) and the buried layer (b) $f_x(x)$, $f_y(x)$, and $f_z(x)$ represent the displacement of a Cu atom along [100], [120], and [001], respectively. For $f_x(x)$, $f_y(x)$, and $f_z(x)$ equal to zero, the model gives 17 Cu atoms for every 16 Ru atoms along [100].

($a = 16a_{\mathrm{Ru}}$). This difference is perhaps not so surprising since the buried layer is in direct contact with the Ru substrate and is, therefore, more affected by the lattice misfit. In any case, the longitudinal modulation is considerably smaller than either transverse modulation.

Interlayer relaxations of the Cu bilayer and the subsequent two Ru layer spacings were also considered in our calculations; however, relaxation of deeper layers did not improve the fit. As shown in Fig. 5, we found that the Cu bilayer contracts on average by 0.3(1)% if the ideal metal radius for Cu is assumed as a reference.[45] The average expansion between the buried Cu layer and the Ru substrate, d_{23}, is 2.5(7)% if the metallic radii for the two species are used.[45] However, the effective spacing between this Cu layer and the Ru surface differs locally due to the Cu corrugation. Taking the corrugation function into account produces a maximum local compression of the Cu film in the Ru hollow sites of 3.5% and a maximum expansion of 4.5% in the bridge sites. These values assume that a Cu atom on a Ru bridge site is 4% elevated in comparison to one in a hollow site (using ideal Cu and Ru metallic radii).[45] We find further that the layer distance d_{34} between the first two Ru layers is compressed by 2.0(2)% and that d_{45} is compressed by 0.7(1)%.

The roughness parameter β was found to be 0.130(4), a value that is reasonable for metal surfaces as defined by Robinson.[34] The introduction of this parameter improves the fit to the CTR significantly, reducing the weighted residual from 4.6% to 3.4%. The root mean squared deviation from the mean of the height-height correlation function, σ_{RMS}, has a value of 0.9 Å,[34] and is related to the step height of the Ru substrate. Our treatment did not include a domain size distribution, thereby assuming a surface roughness that is caused by uncorrelated steps.

The best fit to all the measured data is shown in Figs. 7(a)–7(d). Figure 7(a) compares the calculated intensities of the $(HK0)$ satellite reflections to the measured intensities on a log-log scale. These intensities are most sensitive to the in-plane surface structure and play a central role in its determination. All the data points should fall on the solid line if the model is in perfect agreement with the experiment. As may be seen, the agreement is excellent. The upper inset in Fig. 7(a) displays an electron density contour of the Cu bilayer projected onto a plane. The lower part shows the difference Fourier map using the measured intensities. There are almost no residual features of the electron density distribution, which emphasizes the good agreement of our model with the in-plane superstructure data. For comparison, the open circles in Fig. 7(a) plot the results if the buried Cu layer were pseudomorphic and the top layer modulated. It is clear that the large discrepancies eliminate this model as a possibility.

Figure 7(b) shows the Q_z dependence of the $(1+\delta,1+\delta,2-2\delta,L)$ and $(2\delta,2-\delta,-2-\delta,L)$ superstructure rods between $L=0.2$ and 2.5. The diamonds represent the experimental data and the solidlines are the best fit. The agreement between measurement and calculation is again excellent to within the errors. The dashed line in this figure repeats the prediction of a model with a pseudomorphic Cu interface and modulated top layer.

Figures 7(c) and 7(d) show the CTR data (diamonds) that were simultaneously used in the calculation together with the

TABLE II. Parameters of modulation functions.

	$a_{j,1}$	$a_{j,2}$	$a_{j,3}$	$p_{j,1}$	$p_{j,2}$	$p_{j,3}$
			Top Cu Layer			
x mod., $j=1$	0.0016(4)	0.0035(7)	0.0037(6)	12.62(6)	1.61(4)	3.34(2)
y mod., $j=2$	0.89(1)	−0.007(1)	0	−0.47(5)	−71.4(2)	0
z mod., $j=3$	0.059(8)	0.002(3)	0	0.08(3)	46(2)	0
			Buried Cu layer			
x mod., $j=1$	0.0015(8)	0.0051(4)	0.0032(3)	−0.64(3)	1.53(4)	3.01(3)
y mod., $j=2$	0.093(2)	0.007(1)	0	−0.50(5)	−59.5(3)	0
z mod., $j=3$	0.059(8)	0.002(3)	0	0.08(3)	46(2)	0

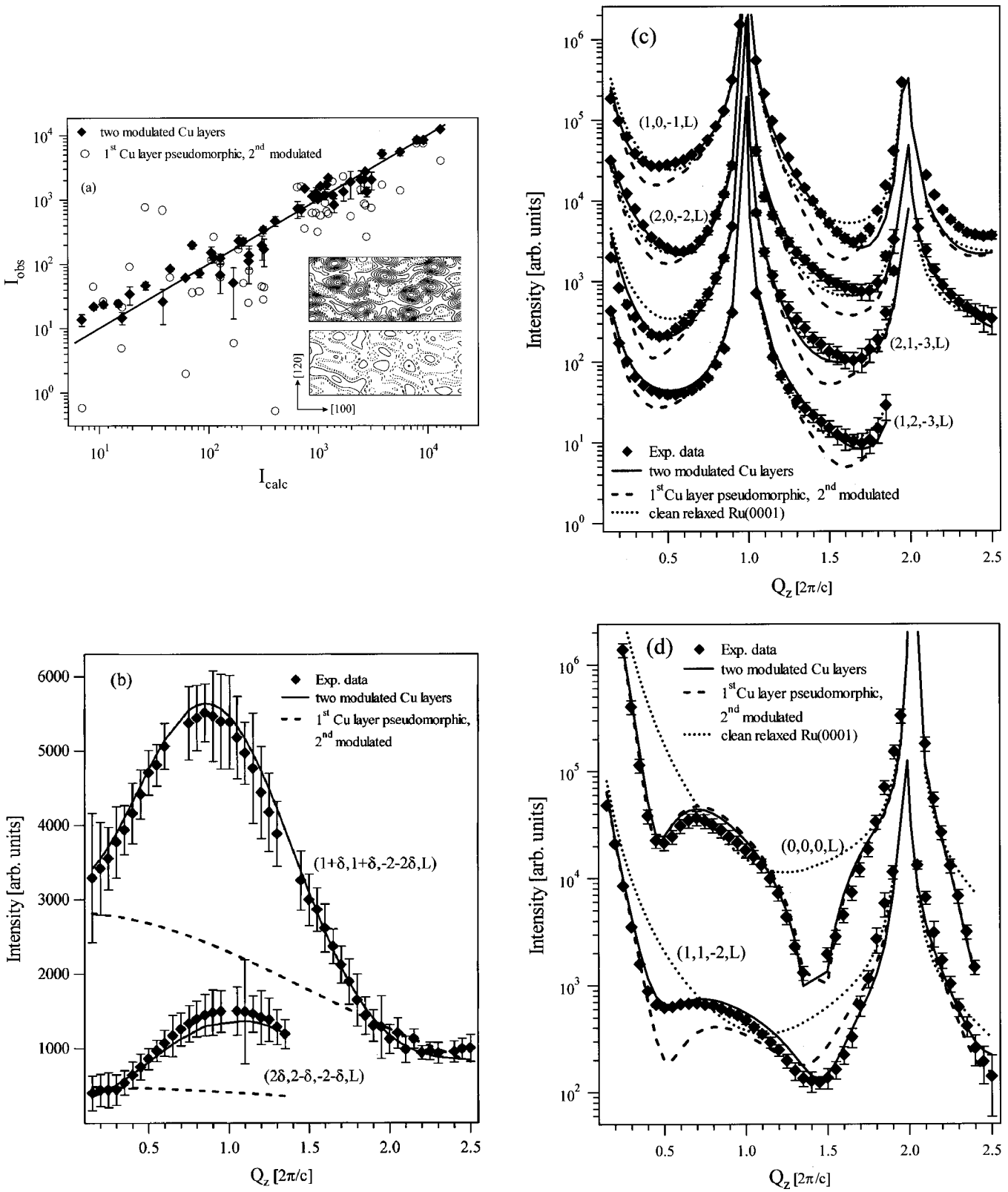

FIG. 7. All experimental SXRD data measured for the stripe phase. The diamond symbols in (a) indicate the agreement of the experimental in-plane intensities (I_{obs}) with the intensities (I_{calc}) derived from the best fit. The upper part of the inset shows an in-plane electron density map of a section of the stripe phase. The lower part shows the difference electron density. The circles show the best fit to a model in which the interfacial Cu layer remains pseudomorphic and only the top Cu layer is reconstructed. (b) shows the agreement between two measured superstructure rods (diamonds) and our best model (solid line). In analogy to (a), the dashed line indicates the intensity distribution for a pseudomorphic buried Cu layer with a modulated Cu layer on top. (c) displays four measured off-specular CTR's of the stripe phase (diamonds) in comparison to our refined model (solid line), a clean, relaxed Ru(0001) surface (dotted line), and a pseudomorphic buried Cu layer with a modulated Cu layer on top (dashed line). In analogy to (c), (d) depicts the $(0,0,0,L)$ together with the $(1,1,-1,L)$ rod.

superstructure data. The measured off-specular rods in Fig. 7(c) are well fitted by our model as can be seen by the solid line. Deviations from the measured data are obvious only for the $(1,0,-1,L)$ rod and for Q_z larger than 1.5. Figure 7(d) shows the $(0,0,0,L)$ and $(1,1,-2,L)$ rods which are also both in good agreement with the experimental intensities. The dotted line in each figure shows the intensity variation calculated for an uncovered, relaxed Ru surface.[36] The differences from the stripe phase are most obvious for the $(0,0,0,L)$ and the $(1,1,-2,L)$ rods [Fig. 7(c)]. The other off-specular rods from a hypothetical clean surface look similar to their equivalents on the reconstructed surface. This is not unexpected since the overlapping amplitudes from the CTR's and the surface reconstruction are very different in strength. The weak satellite reflections produce only a minor phase contrast with the CTR's.

A detailed description of the average Cu modulation functions and vertical layer spacings now allows the strain distribution within the Cu bilayer to be written in terms of the Cu-Cu bond length deviations from their bulk values. Figures 8(a)–8(c) display the deduced Cu-Cu bond lengths as a function of their position along the [100] direction. The insets in these figures represent the respective bond types. Figure 8(a) depicts the three different in-plane bonds lengths of the top Cu layer, Fig. 8(b) shows the equivalent bond types for the buried Cu layer, and Fig. 8(c) portrays the bond length variations between the two Cu layers. The bond errors are of the order of 1.5% and are not displayed. The dashed lines indicate the ideal bulk Cu bond length and serve as a reference for whether a certain Cu-Cu bond at the modulated interface is expanded or compressed.

Figures 8(a) and 8(b) show that the interfacial Cu layer is laterally expanded in the fcc regions and compressed in the hcp regions, relative to bulk Cu. Further, the top Cu layer appears to be less strained in the fcc and hcp stripes than the underlying Cu layer, indicating a negative strain gradient toward the surface. More specifically, it becomes immediately clear from Fig. 8(a) that the bonds connecting parallel modulated Cu rows [$Cu_{1\text{-}3}$,$Cu_{2\text{-}3}$,$Cu_{4\text{-}6}$,$Cu_{5\text{-}6}$ in Figs. 8(a) and 8(b)] are expanded throughout the entire reconstruction by up to 7%. However, in the hcp stacking regions the Cu-Cu in-plane bonds $Cu_{1\text{-}2}$ and $Cu_{4\text{-}5}$ are compressed in the top and buried Cu layers by up to 4.5% and 7%, respectively. These results mirror the fact that the strain relief occurs along [100] and not parallel to the modulated Cu rows. The interplay between strain relief and the preference of Cu atoms for threefold coordination with Ru atoms is apparent in the fcc stacking region of the Cu-Ru interface. There we find that the buried layer is only slightly expanded along [100] (by up to 2.5%), which leads to an optimized Cu coordination at the expense of strain relief. The equivalent $Cu_{1\text{-}2}$ bonds in the top Cu layer are strained differently in this region. They show an average compression of 1% with the maximum in the middle of the fcc stacking area. This implies that the top Cu layer is less strained than the interfacial Cu layer.

We note that the $Cu_{1\text{-}2}$ and $Cu_{4\text{-}5}$ bond lengths change continuously in the dislocation regions. This allows the above mentioned expansion of the Cu bilayer in and at the borders of the fcc region, and leads to the compression in the hcp stacking area. Interlayer Cu-Cu bonds are mostly compressed up to a local maximum of 6% as shown in Fig. 8(c).

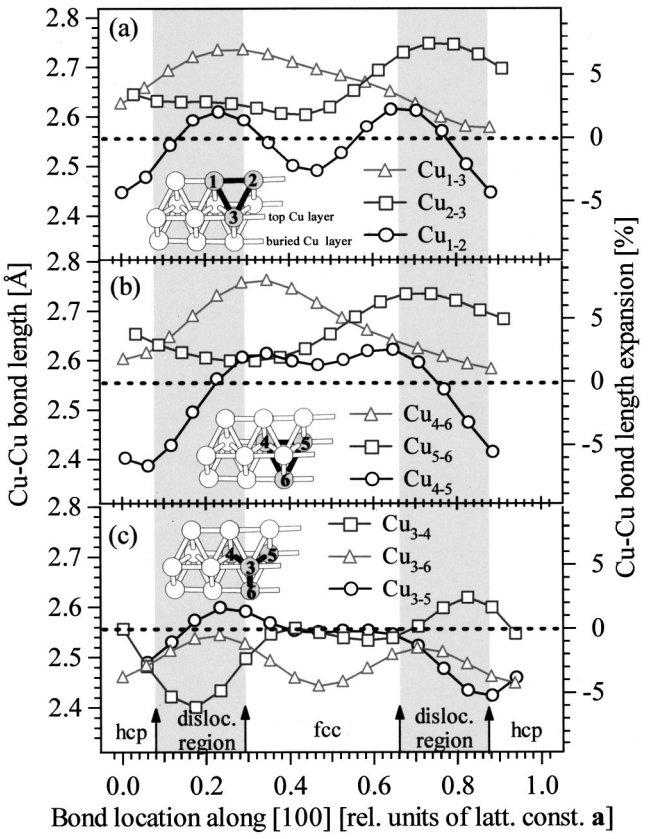

FIG. 8. Cu-Cu bond lengths plotted along the [100] direction. On the left, the ordinate is scaled in angstroms, on the right in units of Cu nearest-neighbor distance. The dashed line in each figure distinguishes Cu compression from expansion. The insets in (a), (b), and (c) define the bond types. (a) displays the in-plane bonds of the top Cu layer, (b) shows the in-plane bonds of the buried Cu layer, and (c) depicts the different bonds between the Cu layers.

However, the deviations of these interlayer bonds from their ideal bulk values are on average smaller than those of the lateral bonds. In addition, it is obvious from Fig. 8(c) that the interlayer bond distances are primarily strained in the dislocation regions of the stripe phase.

Finally, we recall that the symmetry of stripe-phase reconstruction is $P1$ due to the uniaxial modulation of Cu chains along [100]. A higher symmetry in the strain distribution is not expected and not observed. Structurally, a slight lateral displacement of the two Cu layers is indicated by the observed asymmetry in the bond length between the two Cu layers. This results in a distortion of the three fold coordination of Cu atoms at the surface by the underlying layer. For example, the last data point triple in Fig. 8(c) (right side) indicates that atom 3 is displaced in the direction of atoms 5 and 6, making its vertical distance smaller than that to atom 4.

SUMMARY

We have described an x-ray diffraction study of the structure of thin strained Cu films on Ru(0001) at 720 K. We find that a monolayer of Cu is pseudomorphic on Ru(0001) in agreement with earlier studies. The Cu film is, however, highly strained due to the corresponding lattice misfit (5.8%)

with the Ru substrate. Our analysis reveals a 5.95% vertical expansion of the Cu layer calculated with respect to the average ideal metallic radii of Cu and Ru, and a 0.56 to 0.23% compression of the top most Ru-Ru interlayer. Further Cu deposition leads to a stripe phase reconstruction with a 6.25% denser packing in both Cu ad-layers. At 720 K, this occurs through a uniaxial modulation of 17 Cu atoms over 16 Ru atoms along the [100] direction with a $\begin{pmatrix} 16 & 1 \\ 1 & 2 \end{pmatrix}$ superstructure cell. The details of the bilayer reconstruction have been analyzed by applying simulated annealing and least squares refinement techniques to both superstructure and CTR data simultaneously. Our analysis shows that the Cu bilayer consists of two Cu chains which are approximately sinusodially displaced transverse to the [100] direction. Longitudinal displacements of Cu atoms along [100] are small, however, their distribution is strongly asymmetric. The resulting pattern consists of alternating stripes of hcp and fcc stacking of Cu on Ru(0001) as one travels along the [100] direction. These stripes are separated by dislocation regions in which the Cu atoms reside in quasibridge sites. From a detailed study of the bond length distribution in the stripe phase, it can be shown that the interfacial Cu layer is expanded in the fcc regions and compressed in the hcp regions relative to bulk. Further, the top Cu layer appears to be less strained in the fcc and hcp stripes than the underlying Cu layer. Finally, the Ru surface is not modulated by the Cu bilayer, apart from small relaxations of the interlayer spacing near the interface.

ACKNOWLEDGMENTS

We acknowledge many helpful discussions with our colleagues Norm Bartelt, Jose De La Figuera-Bayon, John Hamilton, Bob Hwang, Karsten Pohl, and Andreas Schmidt-.BNL is supported by the U.S. DOE under Contract No. DE-AC02-98CH10886. ORNL is managed by Lockheed Martin Energy Research Corp. under U.S. DOE Contract No. DE-AC05-96OR22464.

*Corresponding author: FAX: 631-344 27 39; Email address: zajonz@bnl.gov

[1] H. Wolter, K. Meinel, Ch. Ammer, K. Wandelt, and H. Neddermeyer, Phys. Rev. B **56**, 15 459 (1997).
[2] K. Meinel, H. Wolter, Ch. Ammer, and H. Neddermeyer, Surf. Sci. **402-404**, 299 (1998).
[3] K. Meinel, H. Wolter, Ch. Ammer, and H. Neddermeyer, Surf. Sci. **401**, 434 (1998).
[4] C. Ammer, K. Meinel, H. Wolter, and H. Neddermeyer, Surf. Sci. **401**, 138 (1998).
[5] A. K. Schmid, N. C. Bartelt, J. C. Hamilton, C. B. Carter, and R. Q. Hwang, Phys. Rev. Lett. **78**, 3507 (1997).
[6] Ch. Ammer, K. Meinel, H. Wolter, and H. Neddermeyer, Surf. Sci. **377-379**, 81 (1997).
[7] Ch. Ammer, K. Meinel, H. Wolter, A. Beckmann, and H. Neddermeyer, Surf. Sci. **375**, 302 (1997).
[8] H. Wolter, K. Meinel, Ch. Ammer, K. Wandelt, and H. Neddermeyer, Surf. Sci. **377-379**, 983 (1997).
[9] J. L. Steven and R. Q. Hwang, Phys. Rev. Lett. **74**, 2078 (1995).
[10] C. Günther, J. Vrijmoeth, R. Q. Hwang, and R. J. Behm, Phys. Rev. Lett. **74**, 754 (1995).
[11] C. B. Carter and R. Q. Hwang, Phys. Rev. B **51**, 4730 (1995).
[12] Ch. Günther, Dissertation, Universität München, 1994.
[13] P. J. Feibelman, J. E. Houston, H. L. Davis, and D. G. O'Neil, Surf. Sci. **302**, 81 (1994).
[14] H. Wolter, M. Schmidt, M. Nohlen, and K. Wandelt, Surf. Sci. **298**, 173 (1993).
[15] G. O. Pötschke and R. J. Behm, Phys. Rev. B **44**, 1442 (1991).
[16] G. O. Pötschke, J. Schröder, C. Günther, R. Q. Hwang, and R. J. Behm, Surf. Sci. **251**, 592 (1991).
[17] C. Park, E. Bauer, and H. Poppa, Surf. Sci. **187**, 86 (1987).
[18] J. E. Houston, C. H. F. Peden, D. S. Blair, and D. W. Goodman, Surf. Sci. **167**, 427 (1986).
[19] K. Christmann, G. Ertl, and H. Shimizu, J. Catal. **61**, 197 (1980).
[20] A. Brown and J. C. Vickerman, Surf. Sci. **140**, 261 (1984).
[21] H. Zajonz, Doon Gibbs, A. P. Baddorf, and D. M. Zehner, Surf. Sci. Lett. **447**, L141 (2000).
[22] J. H. Sinfelt, *Bimetallic Catalysts* (Wiley, New York, 1983).
[23] C. H. F. Peden and D. W. Goodman, J. Catal. **104**, 347 (1987).
[24] J. A. Rodriquez and D. W. Goodman, Surf. Sci. Rep. **14**, 1 (1991).
[25] S. Jansen, M. Palmieri, and S. Lawrence, J. Catal. **163**, 262 (1996).
[26] J. C. Osborne, J. Appl. Phys. **53**, 1586 (1982).
[27] M. Mavrikakis, B. Hammer, and J. K. Nørskov, Phys. Rev. Lett. **81**, 2819 (1998).
[28] M. Gsell, P. Jakob, and D. Menzel, Science **280**, 717 (1998).
[29] J. C. Hamilton and S. M. Foiles, Phys. Rev. Lett. **75**, 882 (1995).
[30] D. Gibbs, B. M. Ocko, D. M. Zehner, and S. G. J. Mochrie, Phys. Rev. B **42**, 7330 (1990).
[31] I. J. Malik and J. Hrbek, J. Phys. Chem. **95**, 2455 (1991).
[32] L. Surney, G. Rangelov, and G. Bliznakov, Surf. Sci. **159**, 299 (1985).
[33] I. K. Robinson, in *Handbook of Synchrotron Radiation*, edited by E. D. Moncton and G. S. Brown (North Holland, Amsterdam, 1990), Vol. 3.
[34] I. K. Robinson, Phys. Rev. B **33**, 3830 (1986).
[35] $R_w(\log_{10}[I]) = \Sigma_{hkl} |\log_{10}(|F^{obs}_{hkl}|^2) - \log_{10}(|F^{calc}_{hkl}|^2)| / \Sigma_{hkl} \log_{10}(|F^{obs}_{hkl}|^2)$, with $|F^{obs}_{hkl}|^2$ the measured intensity and $|F^{calc}_{hkl}|^2$ the calculated intensity.
[36] A. P. Baddorf, H. Zajonz, D. M. Zehner, and Doon Gibbs (unpublished).
[37] *International Tables for X-ray Crystallography*, edited by C. H. Mac Gillavry, G. D. Rieck, and K. Lonsdale (Birmingham, England, 1962), Vol. III, p. 232.
[38] P. J. Feibelman, Surf. Sci. **360**, 297 (1996).
[39] J. E. Houston, C. H. F. Peden, P. J. Feibelman, and D. R. Hamann, Phys. Rev. Lett. **56**, 375 (1986).
[40] J. C. Vickerman, K. Christmann, G. Ertl, P. Heimann, F. J. Himpsel, and D. E. Eastman, Surf. Sci. **134**, 367 (1983).
[41] H. Zajonz, H. L. Meyerheim, T. Gloege, W. Moritz, and D. Wolf, Surf. Sci. **398**, 369 (1998).
[42] Masaaki Korekawa, Habilitationsschrift, Ludwig-Maximilians-Universität München, 1967.
[43] A. L. Ingber, J. Math. Comput. Model **12**, 967 (1989).
[44] A. L. Ingber, Phys. Rev. A **42**, 7057 (1990).
[45] M. E. Straumanis and L. S. Yu, Acta Crystallogr., Sect. A: Cryst. Phys., Diffr., Theor. Gen. Crystallogr. **25A**, 676 (1969).